

Surface Structure and Composition of Au–Rh Bimetallic Nanoclusters on TiO₂(110): A LEIS and STM Study

László Óvári, László Bugyi, Zsolt Majzik, András Berkó, and János Kiss*

Reaction Kinetics Research Laboratory, Chemical Research Center of the Hungarian Academy of Sciences, University of Szeged, Hungary, P.O. Box 168, H-6701 Szeged, Hungary

Received: May 16, 2008; Revised Manuscript Received: August 12, 2008

Gold, rhodium, and their coadsorbed layers were prepared on a nearly stoichiometric titania surface by physical vapor deposition (PVD) and were characterized by low-energy ion scattering (LEIS) and scanning tunneling microscopy (STM). It was found that because of the strong tendency of Au segregation in the Au–Rh bimetallic system, Rh atoms that impinged onto Au clusters pregrown on TiO₂(110) became covered by gold atoms by place exchange or surface diffusion even at room temperature. The incorporation of rhodium led to a slight enlargement of gold clusters indicated by STM and to an increase in the number of Au atoms on the outermost layer of metal clusters evidenced by LEIS. At the same time, separate Rh clusters were also formed on the free oxide surface. The observed effect on the bimetallic nanoclusters is attributed to the different surface free energies of metals. For Au, this value is much smaller than for Rh, which provides a driving force for the bimetallic clusters to be covered by gold atoms. Annealing experiments revealed that monometallic Rh clusters are encapsulated at ~750 K by the oxide. Encapsulation by titania is negligible up to 900 K for the bimetallic nanoparticles almost completely covered by Au.

1. Introduction

In materials science, metal/oxide interfaces can be found in many technological materials, such as functional ceramics with metals, oxide dispersion-strengthened alloys, oxide coatings on metals, and metal–oxide–semiconductor field-effect transistors (MOSFET). Presently, the sizes of many devices and technological materials are rapidly decreasing to the nanoregime. As we approach the nano region, the density of interfaces increases substantially, such that the effect of metal–oxide interactions becomes more and more decisive.¹ The formation of metal nanoparticles on different oxide supports is of great technological importance in catalysis and gas-sensors. TiO₂ is extensively used as a photocatalyst,² and it also has excellent properties as a support material in part because of its reducibility.³ Moreover, it has been established that the electronic interaction with the supported catalyst particles has an important role in determining the effect of semiconductor supports like titania.⁴ It is frequently emphasized that in the wetting of titania, the reactivity of the overlayer metal toward oxygen is one of the decisive factors.⁵ Highly dispersed, oxide- or zeolite-supported bimetallic catalysts are widely used in the catalytic industry, such as in catalytic reforming, nitrogen industry, and gas-to-liquid technology. It is highlighted that in contrast to bulk alloys, nanosized bimetallic systems are extremely sensitive to the structure, morphology, and valence state of the oxide material on which the nanoparticles are prepared.⁶ “Ensemble” or “ligand” effects are frequently invoked to explain the promoting effect of the second metal.^{6,7} The combination of groups VIII B and IB noble metals proved to be beneficial in many cases. The presence of Pd, for example, significantly increased the CO oxidation rate on Au/TiO₂.⁶ Recently, it was established that addition of the unreactive silver enhances the catalytic activity in NO_x decomposition over Rh/Al₂O₃ surfaces.^{8,9}

Moreover, carbon-supported PtAu electrocatalysts showed superior performance as cathodes in direct methanol fuel cells compared to Pt/C cathodes.¹⁰ A gold–rhodium bimetallic core–shell catalyst prepared by a colloidal synthesis was proposed for visible-light-induced hydrogen generation.¹¹

In a recent low-energy ion scattering (LEIS), X-ray photoelectron spectroscopy (XPS), and scanning tunneling microscopy (STM) study, we found that on titania the Mo coadsorption enhanced the Au dispersion (defined, like usually in catalysis as the percentage of gold atoms in the topmost layer, with respect to the total gold content) and led to the disruption of Au nanoparticles.¹² Mo deposition on a nearly stoichiometric TiO₂(110) surface at 300 K caused a remarkable increase in the gold dispersion at larger Au coverages (>0.6 ML) corresponding to the rupture of Au–Au bonds in 3D particles with low kinetic hindrance. The dispersion enhanced irrespective of the deposition sequence of the metals,¹² which was correlated to stronger Au–Mo and Au–TiO_x bond related to the Au–Au bond strength. It was deduced that the strong reactivity of Mo toward titania plays a role in that process.

In the present work, we report on the interaction of gold supported on TiO₂(110) with rhodium, which interacts more weakly with titania^{1,13} mainly because of its lower activity toward surface oxygen. Interestingly, the number of Au atoms on the topmost layer increased also in this case, but the mechanism of the process is different from the Au–Mo bimetallic system.

Details of cluster growth on TiO₂(110) were thoroughly investigated both for gold and rhodium. Earlier studies (reviewed in ref 14) revealed that gold forms “quasi” two-dimensional islands at small coverages ($\Theta_{\text{Au}} \approx 0.1$ ML) with a thickness of one or possibly two atomic layers. The coverage range, characteristic of the 2D growth, was larger (up to $\Theta_{\text{Au}} = 0.2$ ML) when the substrate temperature was low or when the defect density was higher, obtained, for example, by ion sputtering.¹⁵ Oxygen vacancies are the nucleation centers, and it was also

* To whom correspondence should be addressed. Tel/fax: +36-62-420-678; e-mail: jkiss@chem.u-szeged.hu.

demonstrated that the clusters trap several oxygen vacancies beneath them.¹⁶ At higher coverages, 3D growth occurs because of the weak interaction with the support.^{5,14,17} It was demonstrated in our laboratory that on the effect of preadsorbed K, the average size of the gold clusters is significantly smaller at room temperature.¹⁸

Deposition of Rh onto an almost stoichiometric TiO₂(110) surface induced no changes in the Ti 2p XPS feature suggesting a weak interaction with the oxide.^{13,19} However, an electron transfer from Ti³⁺ ions at defect sites to Rh was observed.^{1,13} The 3D rhodium clusters nucleated on the terraces, and step decoration was observed only after annealing to 1100 K.²⁰ A lower substrate temperature (160 K instead of 300 K) during physical vapor deposition of Rh resulted in the growth of smaller clusters.¹⁹ It is well-known that annealing the Rh/TiO₂(110) surface to higher temperatures results in the encapsulation of metal nanoparticles by the oxide depending also on the defect density of the surface region.^{1,13}

2. Experimental Methods

The experiments were performed in two separate ultrahigh vacuum (UHV) systems (base pressure < 5 × 10⁻⁸ Pa). The first one was equipped with facilities for LEIS, auger electron spectroscopy (AES), and XPS measurements (previously described in refs 12, 21, and 22), and in the second one, STM and AES techniques were applied.¹⁸ Two similar rutile TiO₂(110) samples (products of PI-KEM) were parallelly studied in the two pieces of UHV equipment without transferring the probes, and the measurements were cross-calibrated as described below.

A Specs IQE 12/38 ion source was used for LEIS. He⁺ ions of 800 eV kinetic energy were applied at a low ion flux equal to 0.03 μA/cm², which was necessary to avoid the sputtering of surfaces. The incident and detection angles were 50° (with respect to surface normal), while the scattering angle was 95°. The ions and electrons were analyzed by a Leybold hemispherical energy analyzer. The Al Kα X-ray source was an ATOMKI product.²³ The STM measurements were carried out by a commercial room temperature STM head (WA-Technology). The pictures of 256 × 256 pixels were recorded with the bias of +1.5 V (on the sample) and tunneling current of 0.05 nA with an electrochemically etched W-tip. The images were scanned within 3 min on average.

The samples were attached to a Ta plate with a UHV compatible oxide glue (AREMCO, ceramobond 571) and could be heated with a filament placed behind the Ta plate. The sample temperature was measured by a chromel–alumel thermocouple attached to the side of the sample with the same adhesive material. The heating and cooling rates during cleaning and all measurements were less than 2 K/s. The surface was cleaned by 1 keV Ar⁺ ions followed by annealing to 900 K. The cleanliness, composition, and morphology of the surface were controlled by AES, LEIS, XPS, and STM methods.

Rh and Au were deposited by an EGN4 e-beam evaporator of Oxford Applied Research at a substrate temperature of 300 K. The amount of the deposited metals is expressed in equivalent monolayers (eqML) frequently used in literature:^{15,17} 1 eqML is defined as the amount of metal arranged in the close-packed (111) structure required to cover the substrate with a single atomic layer. This quantity is not equal to the fraction of the surface covered by metal, when clusters are higher than one atomic layer. In the STM chamber, the surface concentrations of the deposited metals were estimated from the volume of the nanoparticles separated clearly from each other (usually after a

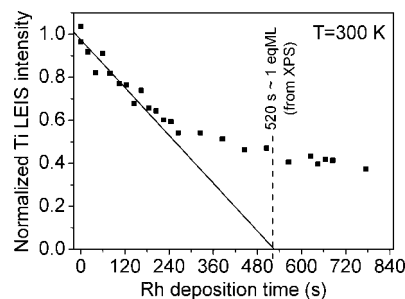


Figure 1. Normalized Ti LEIS intensities as a function of Rh deposition time. The solid straight line is fitted to the LEIS data obtained in the first 180 s. The dashed line is the evaporation time required to deposit 1 eqML of Rh, according to XPS data, assuming a monolayer growth at least up to 120 s (for details see text).

short annealing at higher temperatures). In the other chamber, LEIS and XPS were used for the same purpose. LEIS supplies information only of the outermost atomic layer when performed with noble gas ions.²⁴ The calibration of Au coverage is described in ref 12 while that of Rh is presented below.

3. Results and Discussion

First, we investigated the growth of rhodium nanoparticles on TiO₂ by LEIS focusing on the possibility of a (quasi) 2D initial growth as was observed in the case of gold on TiO₂(110). Deposition of rhodium on TiO₂(110) led to a decrease in the Ti and O LEIS peaks because of the shadowing effect of Rh. The decrease in the Ti (and O) LEIS peak intensities as a function of deposition time was linear up to ~180 s (Figure 1) implying that in this time interval nanoparticles of the same height grew. On the basis of the comparison of XPS and LEIS results, one can determine the layer thickness. Using the Ti 2p, O 1s, and Rh 3d XP peak areas obtained after 120 s of evaporation, assuming a model in which Rh islands with a thickness of one atomic layer (0.22 nm, the distance between Rh(111) sheets) are located on top of the oxide surface, the quantity of rhodium was $\Theta_{\text{Rh}} = 0.23$ eqML. In this calculation, a photoelectric cross section of Scofield²⁵ and inelastic mean free path values of Seah and Dench²⁶ were applied with the help of the XPS Multiquant software.²⁷ It means that 522 s is required to deposit 1 eqML of metal (dashed line in Figure 1). Similarly, assuming a cluster thickness of two and three atomic layers at 120 s, the coverage values obtained from the XPS areas were 0.25 eqML and 0.27 eqML, respectively. Consequently, the evaporation times required to deposit 1 eqML, assuming that initially clusters with a thickness of two and three atomic layers grew, were 480 and 455 s, respectively.

One can see in Figure 1 that the intersection of the straight line (fitted on the LEIS points obtained in the first 180 s) with the *x* axis coincides very well with the deposition time required to achieve one monolayer calculated on the basis of XPS data and assuming an initial layer thickness of one atomic layer. If one assumes, however, that in the linear regime of the Ti LEIS signal decrease the cluster thickness is two atomic layers, then the extrapolation of the straight line fitted on the LEIS data should reach the zero Ti LEIS intensity at 2 eqML. This is, however, in sharp contrast with the XPS measurements, which indicate a deposition time of 960 s, required to deposit 2 eqML of Rh, assuming an initial bilayer growth. The difference between the LEIS and XPS scale is even larger if one assumes a trilayer growth for the first period. Hence, we feel safe to conclude that in the first 180 s predominantly 2D growth occurred producing Rh nanoparticles with a thickness of one

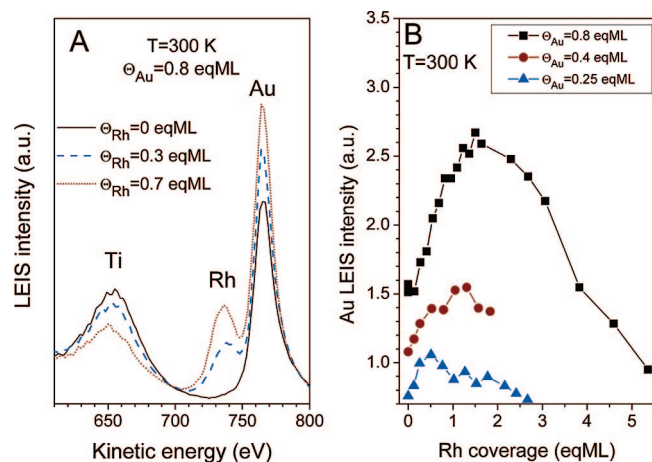


Figure 2. (A) LEIS spectra of the 0.8 eqML Au/TiO₂(110) surface and those obtained after subsequent Rh deposition. (B) LEIS intensities of the Au peak as a function of Rh coverage at different amounts of Au.

atomic layer. Three-dimensional growth started at ~ 0.35 eqML. These observations are in agreement with STM results obtained in the other chamber.

The effect of Rh postdeposition on the Au/TiO₂(110) surface was first investigated by LEIS at room temperature (Figure 2). Deposition of Rh on the 0.8 eqML Au/TiO₂(110) surface led to a decrease in the Ti and O LEIS peaks because of the shadowing effect of Rh. On the contrary, a significant increase in the LEIS signal was detected for Au, which means that the number of Au atoms on the topmost layer was enhanced (Figure 2A) in spite of the fact that a part of rhodium atoms impinged on top of gold clusters during evaporation. It was shown experimentally for different values of the initial gold coverages Θ_{Au} that this behavior is somewhat stronger at higher gold amounts (Figure 2B). On the other hand, a slight increase in the Au signal was also observed when Rh was deposited at $\Theta_{Au} = 0.1$ eqML on quasi 2D gold particles (not shown).

To understand the underlying changes in the atomic structure, STM measurements were also performed. First, 0.6 eqML of gold was evaporated onto titania (Figure 3A). As it can be seen on the STM image of 20×20 nm², the gold clusters are well distinguishable from the titania substrate terrace and from each other. The height of the five to seven largest particles is approximately 0.5–0.7 nm, which indicates two to three atomic layers. The diameter of these Au nanoparticles varies between 2.5 and 3.5 nm. The other smaller particles are one to two layers thick with a diameter of less than 2.5 nm. The size of the Au nanoparticles depended slightly on the stoichiometry of the terraces: on more ordered (1×1) surface phases of TiO₂(110), the size of the particles is larger and their surface concentration is smaller.¹⁸ Accordingly, in these experiments, special attention was paid to the well-ordered (1×1) structure of the TiO₂(110) substrate as well as to the good quality of the STM-tip to minimize the imaging failures caused by the tip–sample shape convolution. Moreover, all the statistical data described below were obtained by the evaluation of numerous similar images (at least 10–15) recorded on the appropriate surface regions. The images presented in Figure 3 are only representative pictures recorded after the different treatments. Figure 3B exhibits the surface morphology, which appeared after the deposition of 0.6 eqML Rh onto the Au-covered surface. Although it is not possible to approach repeatedly the same surface region in our STM, it was relatively easy to find regions where nearly the same amount of larger particles appeared on a 20×20 nm²

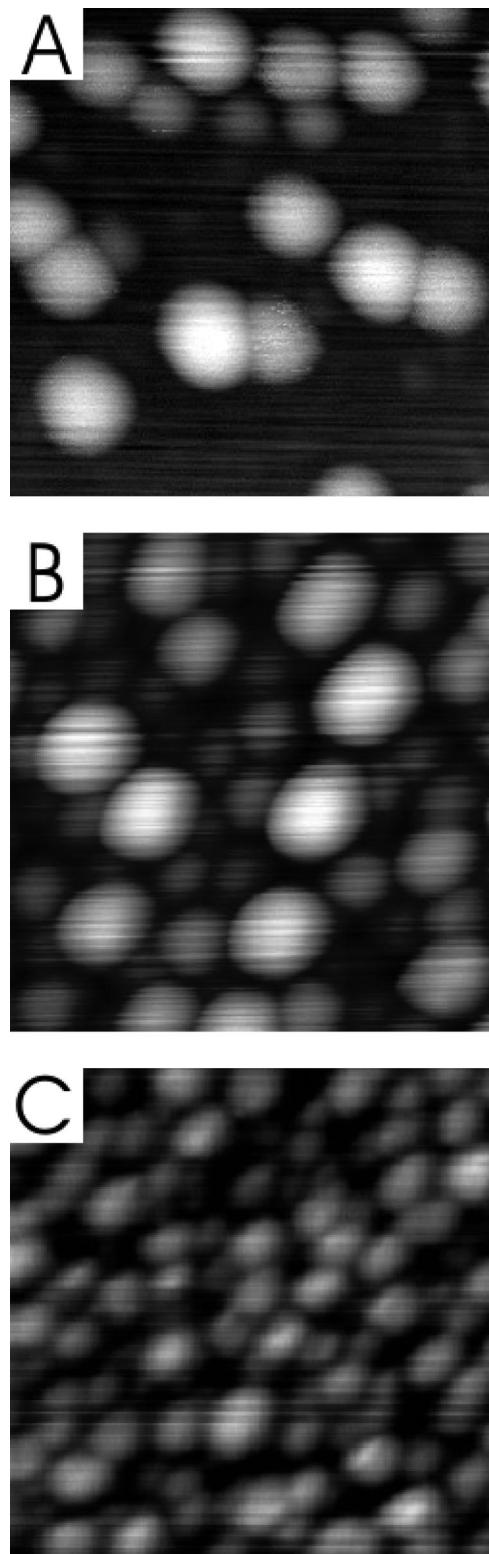


Figure 3. Characteristic STM images of 20×20 nm² recorded on (A) a TiO₂(110) surface deposited by 0.6 eqML of Au at 320–330 K; (B) a surface formed by postdeposition of 0.6 eqML of Rh on the former Au covered surface; and (C) a TiO₂(110) surface deposited by 0.6 eqML of Rh at 320–330 K.

area as after the Au deposition. This behavior indicated for us that the initial larger Au particles can be identified with high reliability. The height of the five to seven outlying particles is in the range of 0.7–0.9 nm with an average diameter of 3–4 nm. Both of these latter parameters are higher by at least 10–20% than that for the initial Au nanoparticles described

above. This fact suggests that the footprint area of these particles increased by 20–40%, while the volume increased at least by 30–50%. By calculating with a simple added Rh layer (0.6 eqML) on two to three layers high Au particles, the increase of the particle volume could not be more than 15–25%. Between the particles of enhanced size, several new particles also can be seen (Figure 3B). These latter ones can be identified as Rh particles nucleated independently from gold on the free TiO₂(110) terraces. The size of these nanoparticles is 1.5–2.0 nm in diameter and 0.2–0.4 nm in height. For comparison, 0.6 eqML of Rh was also deposited on the clean TiO₂(110) surface as shown in Figure 3C. The average size of the Rh nanoparticles formed in this way is similar to those formed among the Au nanoparticles described above.

The enhancement of the Au LEIS peak because of Rh deposition strongly suggests that most of the rhodium atoms, evaporated on top of the gold clusters, moved to subsurface sites of gold particles. The enhanced volume of the bimetallic clusters with the gold atoms outside led to the increase in the LEIS intensity. The strong tendency that the surface of bimetallic clusters is covered by gold instead of rhodium can be rationalized considering that segregation energies show that rhodium does not segregate to the surface of a gold substrate but that gold atoms segregate to Rh surfaces.²⁸ Moreover, the surface free energy of Au is much smaller than that of Rh (at room temperature 1.626 J/m² and 2.828 J/m², respectively²⁹), which again indicates a driving force for the bimetallic clusters to be covered by gold atoms. Gold and rhodium are, on the other hand, immiscible in bulk,³⁰ which implies a preference for phase separation. Though we do not know precisely the energetics of the bonding between Rh and Au atoms in the clusters, the binding energies for the corresponding homo- and heteronuclear diatomic clusters ($D_0^\circ(\text{Rh}_2) = 2.92$ eV, $D_0^\circ(\text{Au}_2) = 2.29$ eV, $D_0^\circ(\text{AuRh}) = 2.37$ eV)³¹ indicate that the Au–Rh bond strength is slightly higher than the Au–Au bond strength, but it is definitely lower than the Rh–Rh bond strength. Similarly, in temperature-programmed desorption (TPD) studies of gold on Rh(111), the multilayer desorption peak was found at somewhat lower temperature than the fractional monolayer peak with the latter being characteristic of the gold–rhodium bonding at 1250 and 1315 K suggesting a desorption activation energy of 3.3 and 3.4 eV, respectively.³² The desorption peak related to the multilayer of Rh on W(211) was found at ~1850 K³³ indicating a desorption activation energy of 4.8 eV, which in agreement with the much stronger Rh–Rh bonding with respect to Au–Rh and Au–Au bonding. It is well-known from literature that also immiscible metals can form bimetallic clusters on oxides, for example, Ru and Cu supported on silica.³⁴ A core–shell structure is realized, in accordance with the tendency for phase separation, with the Cu atoms (having the smaller surface free energy) on the surface. It is reasonable to assume also in our case that the equilibrium distribution of metal atoms would be a Rh-core Au-shell-like structure, but it cannot be completely reached kinetically at room temperature. However, a strong tendency of Au atoms to be located outside is obvious considering the increase in the Au LEIS intensity.

The maximum enhancement of the gold peak was 75% for $\Theta_{\text{Au}} = 0.8$ eqML, while it was only 40% for $\Theta_{\text{Au}} = 0.25$ eqML. A possible reason for this difference is that at higher gold coverages Au clusters are higher, and the fraction of gold atoms located in subsurface position is also larger. For one atomic layer thick Au clusters, one would not expect any gold LEIS intensity enhancement during Rh deposition.

It is possible to estimate more quantitatively whether the incorporation of Rh atoms impinged on top of Au clusters can account for the increase in the Au LEIS intensity. The mean diameter of Au clusters at $\Theta_{\text{Au}} = 0.8$ eqML is 3.4 nm. The thickness of a monolayer of Rh atoms on top of the cluster would be approximately 0.22 nm (the Rh(111) step height), which increases the diameter by 0.44 nm. Rh atoms are assumed to move in subsurface position, but this does not influence considerably the volume. The increase in diameter results in a 30% increase in the cluster footprint area. For a Rh layer with a mean thickness of 1.5 atomic layers, it would be 45%. This value is smaller than the 75% increase which was observed after the deposition of 1.5 eqML of Rh. The somewhat unexpectedly large Au signal increase can be rationalized considering that a fraction of rhodium atoms that landed on the oxide diffuse to Au nanoparticles (they act actually as nucleation centers) and can be trapped and incorporated by gold clusters (trapping mechanism). On the other hand, we do not think that rhodium atoms impinged on the surface of gold clusters would migrate onto the oxide because the interaction of Rh with TiO₂(110) is weak.

In the STM measurements presented above, both gold and rhodium coverages were 0.6 eqML (Figure 3). In the LEIS measurements performed at $\Theta_{\text{Au}} = 0.4$ and 0.8 eqML, the observed Au LEIS intensity enhancement, because of the postdeposition of 0.6 eqML of Rh, was 28% and 33%, respectively (Figure 2B). This is in good agreement with the 20–40% increase in the footprint area of the gold clusters observed by STM. This consistency of the results obtained by the two methods along with the STM data analyzed in connection with Figure 3 further supports our conclusion mentioned above that the trapping mechanism also plays a significant role.

It was observed at all Au coverages investigated that the Au LEIS peak intensity has a maximum at a certain Rh coverage (0.5–1.55 eqML) and that it starts to decrease for higher amounts of Rh (Figure 2B). At $\Theta_{\text{Au}} = 0.8$ eqML, it was larger, however, even after the deposition of 2–3.5 eqML of Rh than the gold intensity observed before Rh deposition. It indicates that the incorporation of Rh atoms, impinged on gold clusters, by Au nanoparticles is very efficient even at room temperature but is not complete (for a more quantitative estimation see below).

A question of kinetic nature still remains: how the encapsulation of Rh atoms by Au is activated. One plausible mechanism is place exchange. A nonthermal place exchange was previously observed even at 30 K, when Rh was deposited on Au(111)³⁵ assuming that the activation energy necessary for the exchange was supplied by the heat of formation of the Rh–Au bond. Migration of Rh into subsurface sites of Au(111) by place exchange could also be induced thermally at 673 K.³⁶ Alternatively, it seems probable that those rhodium atoms on the surface of gold clusters, which do not take part in place exchange, can be covered by Au atoms diffusing on the cluster surface. Both mechanisms involve the incorporation of rhodium into the gold clusters and lead to an increase in the cluster diameter and a concomitant enhancement in the Au LEIS signal. For comparison, it was observed by LEIS in the case of Pt–Rh bimetallic nanoparticles grown at 300 K on TiO₂(110) that the surface becomes Pt rich independent of the deposition order.³⁷ It was taken as evidence that metal atoms can diffuse within the clusters even at room temperature. Similarly, a large amount of Fe was required to coat Pd particles because of the strong tendency of Pd to segregate to the surface of bimetallic particles

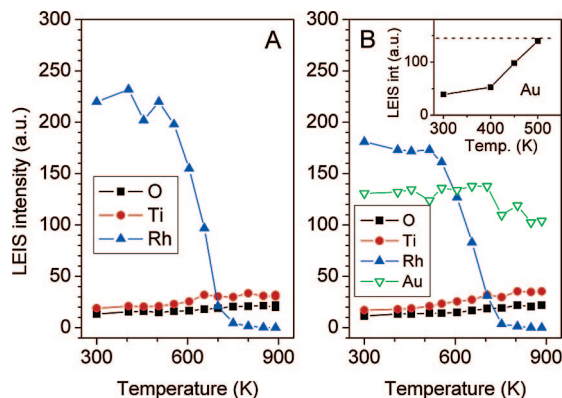


Figure 4. (A) LEIS intensities obtained after the deposition of 1.1 eqML of Rh on TiO₂(110) and the effect of subsequent annealing. (B) LEIS intensities obtained after the deposition of 1.15 eqML of Rh on 0.8 eqML Au/TiO₂(110) and the effect of subsequent annealing. Inset: Au LEIS intensities obtained after the deposition of 5.4 eqML of Rh on 0.8 eqML Au/TiO₂(110) and the effect of subsequent annealing. The dashed line is the maximum Au LEIS intensity, which was possible to reach during Rh deposition (at $\Theta_{\text{Rh}} = 1.9$ eqML) at room temperature on 0.8 eqML Au/TiO₂(110).

during growth at room temperature on alumina.³⁸ Note that the difference in the surface free energies of the constituents is even larger in our case.

In the next measurements, the effect of temperature on the surface composition was investigated by LEIS. Ion scattering intensities after the deposition of 1.1 eqML of Rh on TiO₂(110) at 300 K are displayed in Figure 4A followed by subsequent annealing to higher temperatures. The Rh peak intensity was nearly stable up to ~500 K, and then it steeply decreased and it was almost missing at 800 K and above. The complete disappearance of rhodium signal is a clear sign of encapsulation of Rh nanoparticles by a titanium oxide layer as also previously observed.^{19,37} The agglomeration of Rh clusters is not significant up to 700 K according to STM studies performed in our laboratory.³⁹ The O/Ti LEIS intensity ratio was smaller after the annealing to 900 K than the initially measured value for the clean surface indicating that the encapsulating layer is somewhat reduced.

LEIS intensities obtained after the postdeposition of 1.15 ML of Rh on the 0.8 eqML Au/TiO₂(110) surface at 300 K are shown in Figure 4B followed by annealing to different temperatures. The deposition of Rh led to a 75% increase in the intensity of the Au peak (not shown). This is nearly the maximum intensity enhancement one can reach at this gold coverage during Rh deposition (Figure 2B). Subsequent annealing up to 700 K only resulted in a very slight further enhancement of the gold peak. It indicates that the surface of bimetallic clusters was almost exclusively covered by gold already at room temperature. In case a significant fraction of Rh atoms remained on the topmost layer of bimetallic clusters at room temperature at these coverages, and if there had been gold atoms in subsurface position inside the clusters at 300 K, then a place exchange would have been observed during annealing because of the smaller surface free energy of gold, leading to a further enhancement of Au LEIS signal. The Au intensity increased only by 5% during annealing. Hence, one can estimate that the composition of the outermost layer of bimetallic clusters at 300 K at these coverages was 95% Au and 5% Rh. There are also independent monometallic Rh clusters, as shown by STM (Figure 3B), which are encapsulated at higher temperatures by the oxide, proven by the disappearance of the Rh LEIS intensity at ~750 K (Figure 4B). The presence

of gold, of course, cannot influence the encapsulation of the separate Rh clusters. However, the stability of Au signal up to high temperatures indicates that encapsulation by titania is not significant on these bimetallic particles almost exclusively covered by gold; otherwise, an intensity decrease would occur for the Au peak.

The deposition of Rh on the surface previously covered by gold results in an enhancement of Au LEIS signal only up to a certain Rh coverage, and the evaporation of further amounts of Rh leads to a Au signal decrease indicating the accumulation of Rh also on the topmost layer of bimetallic clusters (Figure 2B). One reason is that there may be no more Au atoms available in subsurface position, which could migrate to the topmost layer. Another reason is that although the encapsulation of Rh by gold at room temperature is quite efficient even at 300 K, it is still somewhat kinetically hindered. It was observed, however, that a slight temperature rise (up to 500 K) is enough to restore the maximum gold intensity even after the deposition of 5.4 ML of Rh (see inset of Figure 4B).

Annealing the surface (0.8 eqML Au + 1.15 eqML Rh on TiO₂(110)) up to 750 K and above led to a gradual decrease in the Au LEIS intensity because of agglomeration (Figure 4B); at 850–900 K, also the desorption of gold may contribute to the intensity loss. The fact that Rh and Au are immiscible suggests that Rh atoms form monometallic clusters inside gold nanoparticles upon thermal activation resulting in a core–shell structure.

4. Conclusions

It was found by LEIS and STM that Rh atoms impinged onto Au clusters grown beforehand on TiO₂(110) were covered by gold atoms through place exchange and surface diffusion already at room temperature. The driving force for the process is related to the surface free energies of the components. At the same time, separate Rh clusters are also formed on the gold free oxide surface. The incorporation of rhodium led to an enlargement of gold clusters and to an increase in the number of Au atoms in the outermost layer of metal clusters evidenced by LEIS and STM. Annealing to higher temperatures did not increase further the number of gold atoms on the topmost layer. Monometallic Rh clusters are encapsulated at ~750 K by the oxide. Encapsulation by titania is negligible up to 900 K for the bimetallic nanoparticles almost completely covered by Au.

Acknowledgment. Support by OTKA NI69327, K69200 and by the National Office for Research and Technology, Pázmány Péter Programme RET-07/2005 is gratefully acknowledged.

References and Notes

- (1) Fu, Q.; Wagner, T. *Surf. Sci. Rep.* **2007**, *62*, 431, and references therein.
- (2) Henderson, M. A.; White, J. M.; Uetsuka, H.; Onishi, H. *J. Am. Chem. Soc.* **2003**, *125*, 14974.
- (3) Grybowska-Świerkosz, B. *Catal. Today* **2006**, *112*, 3, and references therein.
- (4) Solymosi, F. *Catal. Rev.* **1968**, *1*, 233.
- (5) Diebold, U. *Surf. Sci. Rep.* **2003**, *48*, 53, and references therein.
- (6) Guzzi, L. *Catal. Today* **2005**, *101*, 53, and references therein.
- (7) Rodriguez, J. A. *Surf. Sci. Rep.* **1996**, *24*, 223, and references therein.
- (8) Kotsifa, A.; Halkides, T. I.; Kondarides, D. I.; Verykios, X. E. *Catal. Lett.* **2002**, *79*, 113.
- (9) Inderwildi, O. R.; Jenkins, S. J.; King, D. A. *Surf. Sci.* **2007**, *601*, L103.
- (10) Hernández-Fernández, P.; Rojas, S.; Ocón, P.; de Frutos, A.; Figueroa, J. M.; Terreros, P.; Peña, M. A.; Fierro, J. L. G. *J. Power Sources* **2008**, *177*, 9.
- (11) Toshima, N.; Hirakawa, K. *Polym. J.* **1999**, *31*, 1127.

- (12) Bugyi, L.; Berkó, A.; Óvári, L.; Kiss, A. M. *Surf. Sci.* **2008**, *602*, 1650.
- (13) Berkó, A.; Ulrich, I.; Prince, K. C. *J. Phys. Chem. B* **1998**, *102*, 3379.
- (14) Cosandey, F.; Madey, T. E. *Surf. Rev. Lett.* **2001**, *8*, 73, and references therein.
- (15) Parker, S. C.; Grant, A. W.; Bondzie, V. A.; Campbell, C. T. *Surf. Sci.* **1999**, *441*, 10.
- (16) Wahlström, E.; Lopez, N.; Schaub, R.; Thostrup, P.; Rønnow, A.; Africh, C.; Lægsgaard, E.; Nørskov, J. K.; Besenbacher, F. *Phys. Rev. Lett.* **2003**, *90*, 026101.
- (17) Zhang, L.; Persaud, R.; Madey, T. E. *Phys. Rev. B* **1997**, *56*, 10549.
- (18) Kiss, A. M.; Svec, M.; Berkó, A. *Surf. Sci.* **2006**, *600*, 3352.
- (19) Óvári, L.; Kiss, J. *Appl. Surf. Sci.* **2006**, *252*, 8624.
- (20) Berkó, A.; Solymosi, F. *Surf. Sci.* **1998**, *400*, 281.
- (21) Óvári, L.; Kiss, J.; Farkas, A. P.; Solymosi, F. *Surf. Sci.* **2004**, *566*, 1082.
- (22) Óvári, L.; Kiss, J.; Farkas, A. P.; Solymosi, F. *J. Phys. Chem. B* **2005**, *109*, 4638.
- (23) Kövér, L.; Varga, D.; Cserny, I.; Tóth, J.; Tökési, K. *Surf. Interface Anal.* **1992**, *19*, 9.
- (24) Brongersma, H. H.; Draxler, M.; de Ridder, M.; Bauer, P. *Surf. Sci. Rep.* **2007**, *62*, 63, and references therein.
- (25) Scofield, J. H. *J. Electron Spectrosc. Relat. Phenom.* **1976**, *8*, 129.
- (26) Seah, M. P.; Dench, W. A. *Surf. Interface Anal.* **1979**, *1*, 2.
- (27) Mohai, M. *Surf. Interface Anal.* **2004**, *36*, 828.
- (28) Christensen, A.; Ruban, A. V.; Stoltze, P.; Jacobsen, K. W.; Skriver, H. L.; Nørskov, J. K.; Besenbacher, F. *Phys. Rev. B* **1997**, *56*, 5822.
- (29) Mezey, L. Z.; Giber, J. *Jpn. J. Appl. Phys.* **1982**, *21*, 1569.
- (30) Curtarolo, S.; Morgan, D.; Ceder, G. *Comput. Coupling Phase Diagrams Thermochem.* **2005**, *29*, 163.
- (31) Morse, M. D. *Chem. Rev.* **1986**, *86*, 1049.
- (32) Rodriguez, J. A.; Kuhn, M.; Hrbek, J. *J. Phys. Chem.* **1996**, *100*, 3799.
- (33) Pelhos, K.; Abdelrehim, I. M.; Nien, Ch-H.; Madey, T. E. *J. Phys. Chem. B* **2001**, *105*, 3708.
- (34) Sinfelt, J. H. *Acc. Chem. Res.* **1987**, *20*, 134.
- (35) Chado, I.; Scheurer, F.; Bucher, J. P. *Phys. Rev. B* **2001**, *64*, 094410.
- (36) Altman, E. I.; Colton, R. J. *Surf. Sci.* **1994**, *304*, L400.
- (37) Ozturk, O.; Park, J. B.; Ma, S.; Ratliff, J. S.; Zhou, J.; Mullins, D. R.; Chen, D. A. *Surf. Sci.* **2007**, *601*, 3099.
- (38) Felicissimo, M. P.; Martyanov, O. N.; Risse, T.; Freund, H-J. *Surf. Sci.* **2007**, *601*, 2105.
- (39) Berkó, A.; Ménesi, G.; Solymosi, F. *Surf. Sci.* **1997**, *372*, 202.

JP804348M